New Journal of Physics
The open access journal at the forefront of physics

Deutsche Physikalische Gesellschaft DPG IOP Institute of Physics

PAPER • OPEN ACCESS

New self-similar radiation-hydrodynamics solutions in the high-energy density, equilibrium diffusion limit

To cite this article: Taylor K Lane and Ryan G McClarren 2013 *New J. Phys.* **15** 095013

New Journal of Physics
The open access journal for physics

New self-similar radiation-hydrodynamics solutions in the high-energy density, equilibrium diffusion limit

Taylor K Lane and Ryan G McClarren
Department of Nuclear Engineering, Texas A&M University, College Station, TX, USA
E-mail: taylor.lane@neo.tamu.edu and rgm@tamu.edu

New Journal of Physics **15** (2013) 095013 (17pp)
Received 2 April 2013
Published 25 September 2013
Online at http://www.njp.org/
doi:10.1088/1367-2630/15/9/095013

Abstract. This work presents semi-analytic solutions to a radiation-hydrodynamics problem of a radiation source driving an initially cold medium. Our solutions are in the equilibrium diffusion limit, include material motion and allow for radiation-dominated situations where the radiation energy is comparable to (or greater than) the material internal energy density. As such, this work is a generalization of the classical Marshak wave problem that assumes no material motion and that the radiation energy is negligible. Including radiation energy density in the model serves to slow down the wave propagation. The solutions provide insight into the impact of radiation energy and material motion, as well as present a novel verification test for radiation transport packages. As a verification test, the solution exercises the radiation–matter coupling terms and their v/c treatment without needing a hydrodynamics solve. An example comparison between the self-similar solution and a numerical code is given. Tables of the self-similar solutions are also provided.

Contents

1. Introduction

This study deals with a new, self-similar solution to the equations of radiation hydrodynamics (RHD) in the high-energy density regime. In particular it is an extension of the classic Marshak wave problem [1], as solved in detail by Petschek [2]. This problem has been reprised in several monographs that cover RHD [3–5]. The numerical solution of Marshak wave problems was covered in detail by Nelson and Reynolds [6]. It is also worth pointing out that the theory of admissible self-similar solutions is covered in some detail in Coggeshall and Axford [7].

The Marshak wave is a special, soluble problem in RHD, and can arise in high-energy-density experiments where radiation strikes a cold material (e.g. when radiation emitted from a hohlraum strikes a fusion target). As we will demonstrate below, the classical version of this problem is valid in the regime where the radiation energy flux is high, but the radiation energy density is negligible in regard to the material internal energy. Also, the material is considered to be stationary, that is, radiation energy impinges on a quiescent material and drives a radiation wave that travels faster than the speed of sound in the material. Recently, there has been a renewal of interest in RHD solutions. Lowrie and co-workers [8, 9] have published several studies of radiating shock waves using different radiation models, and there has also been developments in the theory of such shocks in different regimes [10–12].

Part of the motivation for these recent papers on RHD behavior has been the necessity of verifying numerical simulation codes for RHD. Verification in this sense means demonstrating that the code is solving the intended equations and that numerical errors behave as expected (e.g. going to zero at the correct rate as the mesh is refined). Our solutions below, besides their inherent interest as novel solutions, can be used to this end in the verification of the radiation–matter coupling part of a simulation code. Our solutions can be used in code verification, regardless of the radiation transport model employed in the code (e.g. flux-limited diffusion, discrete ordinates, Monte Carlo, etc) because our solution is given in the equilibrium diffusion limit, an asymptotic limit of the RHD equations that is possessed by nearly all approximate transport models [13–16].

In the following section we review our RHD model and then derive the equilibrium diffusion model. In section 4 we pose the problem of radiation impinging on a cold slab and present an approach to estimating the location of the wavefront. Solution profiles are evaluated

in section 5, and we demonstrate the usefulness of these solutions for code verification in section 6.

2. Radiation hydrodynamics model

We begin with the equations for RHD as given by Lowrie and Morel previously [17]. The hydrodynamics equations, in non-dimensional form under the condition of local thermodynamic equilibrium [5] are

$$\frac{\partial \rho}{\partial t} + \nabla \cdot (\rho \vec{v}) = 0\,, \tag{1a}$$

$$\frac{\partial}{\partial t}(\rho \vec{v}) + \nabla \cdot (\rho \vec{v} \otimes \vec{v}) + \nabla p = -\mathbb{P}\vec{S}_{\mathrm{F}}\,, \tag{1b}$$

$$\frac{\partial}{\partial t}(\rho E) + \nabla \cdot [(\rho E + p)\vec{v}] = -\mathbb{P}\mathbb{C}S_{\mathrm{E}}\,, \tag{1c}$$

where ρ is the material density, $\vec{v}$ is the relative velocity and p is the pressure. E, the total specific energy is given by

$$E = e + \tfrac{1}{2}v^2, \tag{2}$$

where $v = |\vec{v}|$ and e is the internal specific energy with a simple equation of state $e = c_v T$. The specific heat, c_v, is a uniform and constant parameter. The non-dimensionalization we use as

$$\hat{x} = xl, \qquad \hat{t} = tl/a_\infty, \quad \hat{\rho} = \rho\rho_\infty, \quad \hat{v} = va_\infty,$$
$$\hat{p} = p\rho_\infty a_\infty^2 \quad \hat{T} = TT_\infty \quad \hat{\sigma}_{\mathrm{a}} = \sigma/l, \quad \hat{e} = a_\infty^2 e, \quad \hat{c}_v = c_v c_{\mathrm{v}\infty},$$

where hatted variables are dimensional, l is a characteristic length scale, ρ_∞ is a characteristic density and T_∞ is a reference temperature. The reference sound speed, a_∞, is given using the constant, reference specific heat $c_{\mathrm{v}\infty}$ as

$$a_\infty = \sqrt{c_{\mathrm{v}\infty} T_\infty}. \tag{3}$$

Also, in our model we have included the non-dimensional parameters

$$\mathbb{C} = \frac{c}{a_\infty} = \frac{c}{\sqrt{c_{\mathrm{v}\infty} T_\infty}}, \qquad \mathbb{P} = \frac{a_{\mathrm{r}} T_\infty^4}{\rho_\infty a_\infty^2} = \frac{a_{\mathrm{r}} T_\infty^3}{\rho_\infty c_{\mathrm{v}\infty}}, \tag{4}$$

where c is the speed of light and $a_{\mathrm{r}} = 4\sigma_{\mathrm{SB}}/c$ is the radiation constant with σ_{SB} the Stefan–Boltzmann constant. The interpretation of these parameters is as follows: $\mathbb{C}$ is a measure of how relativistic the flow is and $\mathbb{P}$ is a measure of how much energy is in the radiation field compared with the material internal energy.

In particular, equations (1*a*)–(1*c*) represent the conservation of mass, momentum and energy of the fluid, respectively. We have yet to define the momentum and energy sources in these equations. Before doing so we will introduce the radiation model.

For the radiation transport we will employ a P_1 model [17, 18] that uses a $P_{\mathrm{r}} = E_{\mathrm{r}}/3$ closure model:

$$\frac{\partial E_{\mathrm{r}}}{\partial t} + \mathbb{C}\nabla \cdot \vec{F}_{\mathrm{r}} = \mathbb{C}S_{\mathrm{E}}, \tag{5a}$$

$$\frac{\partial \vec{F}_{\mathrm{r}}}{\partial t} + \frac{1}{3}\mathbb{C}\nabla E_{\mathrm{r}} = \mathbb{C}\vec{S}_{\mathrm{F}}, \tag{5b}$$

where

$$S_{\mathrm{E}} = \sigma(T^4 - E_{\mathrm{r}}) + \sigma\frac{\vec{v}}{\mathbb{C}} \cdot \vec{F}_{\mathrm{r0}}, \tag{6a}$$

$$\vec{S}_{\mathrm{F}} = -\sigma\vec{F}_{\mathrm{r0}} + \sigma\frac{\vec{v}}{\mathbb{C}}(T^4 - E_{\mathrm{r}}), \tag{6b}$$

$$\vec{F}_{\mathrm{r0}} = \vec{F}_{\mathrm{r}} - \left(\vec{v}E_{\mathrm{r}} + \frac{\vec{v}}{3}E_{\mathrm{r}}\right)/\mathbb{C}. \tag{6c}$$

The non-dimensionalization used here has

$$\hat{E}_{\mathrm{r}} = a_{\mathrm{r}}T_{\infty}^4 E_{\mathrm{r}}, \quad \hat{\vec{F}}_{\mathrm{r}} = ca_{\mathrm{r}}T_{\infty}^4\vec{F}_{\mathrm{r}}.$$

In these equations E_{r} is known as the radiation energy density and it is proportional to the zeroth angular moment of the radiation specific intensity. F_{r} is known as the radiation flux and it is proportional to the first angular moment of the radiation specific intensity. The material absorption opacity (with units of inverse scale length) is given by σ. For convenience we have ignored scattering in our radiation transport model.

3. Asymptotic analysis of radiation model

In typical applications the RHD model (i.e. the coupled Euler and radiation equations) are solved in an operator split fashion where the P_1 equations (or some other transport model) is solved coupled with a material internal energy equation that contains the radiation–matter coupling terms only:

$$\frac{\partial\rho e}{\partial t} = -\mathbb{P}\mathbb{C}S_{\mathrm{E}}. \tag{7}$$

The other terms in the material energy equation are updated during the hydrodynamics solve, along with a correction to take into account momentum exchange. As part of the operating splitting procedure, the radiation solve is undertaken with the density and velocity terms evaluated at a particular time level. It is these radiation equations with a quasi-static material velocity and density that we will perform an asymptotic analysis on.

Consider a small, positive parameter ϵ. The P_1 equations above, coupled to equation (7), are to be scaled under the conditions that the absorption cross-section is very large:

$$\sigma \to \frac{\sigma}{\epsilon}$$

and where the ratio of the speed of light to the speed of sound is also very large:

$$\mathbb{C} \to \frac{\mathbb{C}}{\epsilon}.$$

These substitutions indicate that we are considering asymptotic solutions to the transport equation for a system where the absorption opacity is large compared to our reference length scale and the material reacts much quicker to changes in radiation than any material effects such as sound waves.

Substituting these relationships into the P_1 equations and equation (7) gives

$$\epsilon \frac{\partial E_\mathrm{r}}{\partial t} + \mathbb{C}\nabla \cdot \vec{F}_\mathrm{r} = \mathbb{C} S_\mathrm{E}, \tag{8a}$$

$$\epsilon \frac{\partial \vec{F}_\mathrm{r}}{\partial t} + \frac{1}{3}\mathbb{C}\nabla E_\mathrm{r} = \mathbb{C}\vec{S}_\mathrm{F}, \tag{8b}$$

$$\epsilon \frac{\partial \rho e}{\partial t} = -\mathbb{P}\mathbb{C} S_\mathrm{E}, \tag{8c}$$

where the sources are now given by

$$S_\mathrm{E} = \frac{\sigma}{\epsilon}\left(T^4 - E_\mathrm{r}\right) + \sigma \frac{\vec{v}}{\mathbb{C}} \cdot \vec{F}_\mathrm{r0}\,, \tag{9a}$$

$$\vec{S}_\mathrm{F} = -\frac{\sigma}{\epsilon}\vec{F}_\mathrm{r0} + \sigma \frac{\vec{v}}{\mathbb{C}}\left(T^4 - E_\mathrm{r}\right)\,, \tag{9b}$$

$$\vec{F}_\mathrm{r0} = \vec{F}_\mathrm{r} - \frac{\epsilon}{\mathbb{C}}\left(\vec{v}E_\mathrm{r} + \frac{\vec{v}}{3}E_\mathrm{r}\right)\,. \tag{9c}$$

All dependent variables, (E_r, $\vec{F}_\mathrm{r}$ and T), in equations (8*a*)–(8*c*) are now expanded with a formal power series of the scaling constant ϵ. For example

$$E_\mathrm{r} = \sum_{n=0}^{\infty} \epsilon^n E_\mathrm{r}^{(n)}, \quad T^4 = \sum_{n=0}^{\infty} \epsilon^n T_{(n)}^4.$$

We will now look at the coefficients for each power of ϵ. The three orders of S_E are

$$S_\mathrm{E}^{(-1)} = \sigma\left(T_{(0)}^4 - E_\mathrm{r}^{(0)}\right), \tag{10a}$$

$$S_\mathrm{E}^{(0)} = \sigma\left(T_{(1)}^4 - E_\mathrm{r}^{(1)}\right) + \sigma \frac{\vec{v}}{\mathbb{C}} \cdot \vec{F}_\mathrm{r0}^{(0)}, \tag{10b}$$

$$S_\mathrm{E}^{(1)} = \sigma\left(T_{(2)}^4 - E_\mathrm{r}^{(2)}\right) + \sigma \frac{\vec{v}}{\mathbb{C}} \cdot \vec{F}_\mathrm{r0}^{(1)}. \tag{10c}$$

Similarly for S_F:

$$\vec{S}_\mathrm{F}^{(-1)} = -\sigma \vec{F}_\mathrm{r0}^{(0)}, \tag{11a}$$

$$\vec{S}_\mathrm{F}^{(0)} = -\sigma \vec{F}_\mathrm{r0}^{(1)} + \sigma \frac{\vec{v}}{\mathbb{C}}\left(T_{(0)}^4 - E_\mathrm{r}^{(0)}\right), \tag{11b}$$

$$\vec{S}_\mathrm{F}^{(1)} = -\sigma \vec{F}_\mathrm{r0}^{(2)} + \sigma \frac{\vec{v}}{\mathbb{C}}\left(T_{(1)}^4 - E_\mathrm{r}^{(1)}\right). \tag{11c}$$

After inspecting equations (8*a*)–(8*c*), it can be seen that no terms involve ϵ^{-1}. This shows that the $O(\epsilon^{-1})$ equations are equal to zero, therefore $S_\mathrm{E}^{(-1)} = \vec{S}_\mathrm{F}^{(-1)} = 0$. Because of this, equation (10*a*) gives

$$T_{(0)}^4 = E_\mathrm{r}^{(0)} \tag{12}$$

and equation (11*a*) gives

$$\vec{F}_\mathrm{r0}^{(0)} = 0. \tag{13}$$

Gathering only the terms involving no power of ϵ in the P_1 equations, also known as $O(1)$ equations, is as follows:

$$\mathbb{C}\nabla\cdot\vec{F}_{\mathrm{r}}^{(0)} = \mathbb{C}S_{\mathrm{E}}^{(0)}, \tag{14a}$$

$$\tfrac{1}{3}\mathbb{C}\nabla E_{\mathrm{r}}^{(0)} = \mathbb{C}\vec{S}_{\mathrm{F}}^{(0)}, \tag{14b}$$

$$\vec{F}_{\mathrm{r0}}{}^{(0)} = \vec{F}_{\mathrm{r}}^{(0)} = 0. \tag{14c}$$

Equation (14*a*) reduces to $S_{\mathrm{E}}^{(0)} = 0$ due to equation (14*c*). Furthermore, this simplifies equation (10*b*) to

$$T_{(1)}^4 = E_{\mathrm{r}}^{(1)}. \tag{15}$$

The first-order equation for $\vec{F}_{\mathrm{r0}}$ is

$$\vec{F}_{\mathrm{r0}}{}^{(1)} = \vec{F}_{\mathrm{r}}^{(1)} - \frac{1}{\mathbb{C}}\left[\vec{v}E_{\mathrm{r}}^{(0)} + \frac{\vec{v}}{3}E_{\mathrm{r}}^{(0)}\right]. \tag{16}$$

Substituting this relationship and equation (11*b*) into equation (14*b*) gives

$$\frac{1}{3}\nabla E_{\mathrm{r}}^{(0)} = -\sigma\vec{F}_{\mathrm{r}}^{(1)} + \frac{4}{3}\frac{\vec{v}}{\mathbb{C}}\sigma E_{\mathrm{r}}^{(0)} \tag{17}$$

after some algebra. Solving for $\vec{F}_{\mathrm{r}}^{(1)}$ provides a version Fick's Law, relating the radiation flux to the gradient of the energy density, with an additional drift term

$$\vec{F}_{\mathrm{r}}^{(1)} = \frac{4}{3}\frac{\vec{v}}{\mathbb{C}}E_{\mathrm{r}}^{(0)} - \frac{1}{3\sigma}\nabla E_{\mathrm{r}}^{(0)}. \tag{18}$$

Next, we look at the $O(\epsilon)$ equations arising from equations (8*a*)–(8*c*):

$$\frac{\partial E_{\mathrm{r}}^{(0)}}{\partial t} + \mathbb{C}\nabla\cdot\vec{F}_{\mathrm{r}}^{(1)} = \mathbb{C}S_{\mathrm{E}}^{(1)}, \tag{19a}$$

$$-\frac{1}{\mathbb{P}}\frac{\partial\rho e^{(0)}}{\partial t} = \mathbb{C}S_{\mathrm{E}}^{(1)}. \tag{19b}$$

Substituting equation (18) into equation (19*a*) gives

$$\frac{\partial E_{\mathrm{r}}^{(0)}}{\partial t} + \frac{1}{3}\nabla\cdot\left[4\vec{v}E_{\mathrm{r}}^{(0)} - \frac{\mathbb{C}}{\sigma}\nabla E_{\mathrm{r}}^{(0)}\right] = \mathbb{C}S_{\mathrm{E}}^{(1)}. \tag{20}$$

Subtracting equation (19*b*) from equation (20) and rearranging gives

$$\frac{1}{\mathbb{P}}\frac{\partial\rho e^{(0)}}{\partial t} + \frac{\partial E_{\mathrm{r}}^{(0)}}{\partial t} + \frac{4}{3}\nabla\cdot\vec{v}E_{\mathrm{r}}^{(0)} = \nabla\cdot\frac{\mathbb{C}}{3\sigma}\nabla E_{\mathrm{r}}^{(0)}. \tag{21}$$

Finally, this can be given in terms of material temperature due to equation (12) and our equation of state:

$$\frac{\partial\rho c_v T^{(0)}}{\partial t} + \mathbb{P}\frac{\partial T_{(0)}^4}{\partial t} + \mathbb{P}\frac{4}{3}\nabla\cdot\vec{v}\,T_{(0)}^4 = \nabla\cdot\frac{\mathbb{C}\mathbb{P}}{3\sigma}\nabla T_{(0)}^4. \tag{22}$$

For a known density and material velocity (as in the case of an operator split solution), the only dependent variable in this equation is the material temperature. This equation is the equilibrium drift-diffusion limit. The drift term would be absent without material motion. Though we derived these equations starting from a P_1 model for radiation transport, previous asymptotic analyses show that equilibrium diffusion is the asymptotic limit of the most general transport model [19].

4. The problem of radiation impinging on a cold slab

We will now consider equation (22) in one-dimensional slab geometry with constant c_v and an opacity dependent on temperature to some power. This makes equation (22), dropping the (0)'s,

$$\frac{\partial \rho c_v T}{\partial t} + \mathbb{P}\frac{\partial T^4}{\partial t} + \mathbb{P}\frac{4}{3}\frac{\partial}{\partial x} v T^4 = \frac{\partial}{\partial x} \cdot \frac{\mathbb{C}\mathbb{P}}{3\sigma}\frac{\partial}{\partial x} T^4. \tag{23}$$

We note that our model equation, equation (23), can be simplified to the equation solved in several previous studies of Marshak waves [2, 4, 6, 20]. Those studies consider problems where $\mathbb{P}$ is negligibly small and the quantity $\mathbb{C}\mathbb{P} = 1$. It is interesting that one need not assume that $v = 0$ to arrive at the standard Marshak wave solution, only that $\mathbb{P}$ is negligible.

The problem we will solve has an initially cold, semi-infinite material located at $x \geqslant 0$. At time $t = 0$ a radiation source is turned on at $x = 0$, heating the material there to a temperature of $T = 1$. We obtain a self-similar solution to this problem with the similarity transformations

$$\xi = \frac{Ax}{\sqrt{t}}, \quad u(t) = \frac{\theta U}{\sqrt{t}},$$

where A and U are constants to be defined later and θ is a parameter that gives the magnitude of the material velocity, ξ is the scaled independent variable and u is the scaled material velocity. Note that we have prescribed the relationship between the independent variables x and t, and prescribed a form for the material velocity. We do not consider how such a form for the velocity might be formed, rather we assert that if the velocity has such a $1/\sqrt{t}$ dependence our self-similar solutions are possible. Also, the material velocity is constant in space and is only a function of time.

Implementing these transforms results in

$$-\xi\frac{\mathrm{d}}{\mathrm{d}\xi}\left(\rho e + \mathbb{P}T^4\right) + \frac{8}{3}AU\theta\mathbb{P}\frac{\mathrm{d}}{\mathrm{d}\xi}T^4 = \frac{2A^2\mathbb{C}\mathbb{P}}{3}\frac{\mathrm{d}}{\mathrm{d}\xi}\frac{1}{\sigma}\frac{\mathrm{d}}{\mathrm{d}\xi}T^4. \tag{24}$$

Formally introducing the temperature-dependent cross section

$$\sigma = \kappa_0 T^{-n} \tag{25}$$

and substituting into equation (23), and setting $\rho c_v = 1$ gives

$$-\xi\frac{\mathrm{d}}{\mathrm{d}\xi}\left(T + \mathbb{P}T^4\right) + \frac{8}{3}AU\theta\mathbb{P}\frac{\mathrm{d}}{\mathrm{d}\xi}T^4 = \frac{8A^2\mathbb{C}\mathbb{P}}{3(n+4)\kappa_0}\frac{\mathrm{d}^2}{\mathrm{d}\xi^2}T^{(n+4)}. \tag{26}$$

At this point the following constants will be defined to simplify the arithmetic:

$$A^2 = \frac{3(n+4)\kappa_0}{8\mathbb{C}\mathbb{P}}, \tag{27}$$

$$U = \frac{3}{8A} = \left[\frac{3\mathbb{C}\mathbb{P}}{8(n+4)\kappa_0}\right]^{1/2}. \tag{28}$$

Using these relationships, equation (26) simplifies to

$$-\xi\frac{\mathrm{d}}{\mathrm{d}\xi}\left(T + \mathbb{P}T^4\right) + \mathbb{P}\theta\frac{\mathrm{d}}{\mathrm{d}\xi}T^4 = \frac{\mathrm{d}^2}{\mathrm{d}\xi^2}T^{(n+4)}. \tag{29}$$

Once again we point out that this equation in the limit $\mathbb{P} \to 0$ is equivalent to the classical Marshak wave result.

We will solve equation (29) with the boundary condition that $T(0) = 1$ and the condition that the temperature in front of the wave is cold (i.e. $T = 0$). We refer to the value of ξ beyond which $T = 0$ as $\xi_{\max}$. For a particular value of $\xi_{\max}$, there are an infinite number of solutions that tend to zero. However, only one of these solutions maintains a zero flux in the limit $\xi \to \xi_{\max}$. Castor [4] outlines an iterative numerical procedure beginning with an initial guess for $\xi_{\max}$ to determine the wave temperature profile. This value for $\xi_{\max}$ must be adjusted through trial and error until an integration from $\xi_{\max}$ back to 0 gives $T(0) = 1$.

4.1. An approximation to $\xi_{\max}$

To find the $\xi_{\max}$ we begin by integrating both sides of equation (29) over $\xi < \xi' < \xi_{\max}$, giving

$$-\xi\left(T(\xi')+\mathbb{P}T^4(\xi')\right)\Big|_{\xi}^{\xi_{\max}} + \int_{\xi}^{\xi_{\max}} \left(T(\xi')+\mathbb{P}T^4(\xi')\right)\,\mathrm{d}\xi' + \mathbb{P}\theta T^4(\xi')\Big|_{\xi}^{\xi_{\max}} = \frac{\mathrm{d}}{\mathrm{d}\xi}T^{(n+4)}(\xi')\Big|_{\xi}^{\xi_{\max}}. \tag{30}$$

Simplifying using $T(\xi_{\max}) = 0$ yields

$$\xi\left(T(\xi)+\mathbb{P}T^4(\xi)\right) + \int_{\xi}^{\xi_{\max}} \left(T(\xi')+\mathbb{P}T^4(\xi')\right)\,\mathrm{d}\xi' - \mathbb{P}\theta T^4(\xi) = -\frac{\mathrm{d}}{\mathrm{d}\xi}T^{(n+4)}(\xi). \tag{31}$$

For conciseness, the function $g(\xi) = T(\xi) + \mathbb{P}T^4(\xi)$ is defined. From this, the mean value of $g(\xi)$ from ξ to $\xi_{\max}$ can also be defined as

$$\bar{g}(\xi) = \frac{1}{\xi_{\max}-\xi}\int_{\xi}^{\xi_{\max}} g(\xi')\,\mathrm{d}\xi'. \tag{32}$$

Using this relationship allows one to write the first two terms of equation (31) as

$$\xi g(\xi) + \int_{\xi}^{\xi_{\max}} g(\xi')\,\mathrm{d}\xi' = \xi_{\max} g(\xi) - (\xi_{\max}-\xi)\left(g(\xi)-\bar{g}(\xi)\right). \tag{33}$$

Then, due to the fact that $(\xi_{\max} - \xi) \ll \xi_{\max}$ near the radiative wave front, the second term can be neglected. Therefore, equation (33) reduces to

$$\xi g(\xi) + \int_{\xi}^{\xi_{\max}} g(\xi')\,\mathrm{d}\xi' \approx \xi_{\max} g(\xi). \tag{34}$$

Nelson and Reynolds illustrate the previous approximation in [6, equations (6), (7)] and state that the relative error is of order $(\xi_{\max} - \xi)/\xi_{\max}$. Modulo this error, equation (31) reduces to

$$\xi_{\max}[T(\xi)+\mathbb{P}T^4(\xi)] - \mathbb{P}\theta T^4(\xi) = -\frac{\mathrm{d}}{\mathrm{d}\xi}T^{(n+4)}(\xi). \tag{35}$$

Notice that through the chain rule

$$(n+4)T^{(n+3)}(\xi)\frac{\mathrm{d}}{\mathrm{d}\xi}T(\xi) = \frac{\mathrm{d}}{\mathrm{d}\xi}T^{(n+4)}(\xi). \tag{36}$$

Because of this, equation (35) can be rewritten as

$$\xi_{\max}[T(\xi)+\mathbb{P}T^4(\xi)] - \mathbb{P}\theta T^4(\xi) = -(n+4)T^{(n+3)}(\xi)\frac{\mathrm{d}}{\mathrm{d}\xi}T(\xi). \tag{37}$$

Dividing both sides by $T(\xi)$ gives

$$\xi_{\max}[1+\mathbb{P}T^3(\xi)]-\mathbb{P}\theta T^3(\xi)=-(n+4)T^{(n+2)}(\xi)\frac{\mathrm{d}}{\mathrm{d}\xi}T(\xi). \tag{38}$$

Now, applying a reverse application of the chain rule gives

$$\xi_{\max}[1+\mathbb{P}T^3(\xi)]-\mathbb{P}\theta T^3(\xi)=-\frac{(n+4)}{(n+3)}\frac{\mathrm{d}}{\mathrm{d}\xi}T^{(n+3)}(\xi). \tag{39}$$

This reduces to

$$\xi_{\max}+[\xi_{\max}-\theta]\,\mathbb{P}T^3(\xi)=-\frac{(n+4)}{(n+3)}\frac{\mathrm{d}}{\mathrm{d}\xi}T^{(n+3)}(\xi). \tag{40}$$

A final integration over ξ and again taking advantage of the fact that $T(\xi_{\max})=0$ gives

$$\xi_{\max}(\xi_{\max}-\xi)+\mathbb{P}\,[\xi_{\max}-\theta]\int_{\xi}^{\xi_{\max}}T^3(\xi')\,\mathrm{d}\xi'=\frac{(n+4)}{(n+3)}T^{(n+3)}(\xi). \tag{41}$$

Furthermore, evaluating the remaining integral using right-hand Riemann sums yields

$$\int_{\xi}^{\xi_{\max}}T^3(\xi')\,\mathrm{d}\xi'=(\xi_{\max}-\xi)T^3(\xi_{\max})=0 \tag{42}$$

due to $T^3(\xi_{\max})=0$. This method maintains accuracy to order $(\xi_{\max}-\xi)/\xi_{\max}$. Equation (41) now reduces to

$$\xi_{\max}\,(\xi_{\max}-\xi)=\frac{(n+4)}{(n+3)}T^{(n+3)}(\xi). \tag{43}$$

Solving this equation for $T(\xi)$ provides an initial temperature approximation which is defined as $T_1(\xi)$:

$$T_1(\xi)=\left[\frac{(n+3)}{(n+4)}\xi_{\max}\,(\xi_{\max}-\xi)\right]^{1/(n+3)}. \tag{44}$$

With this temperature approximation we can evaluate the integral in equation (41) instead of using right-hand Riemann sums. This will generate a more accurate expression in which we will explicitly solve for $T(\xi)$ below. Substituting $T_1(\xi)$ into the integral term gives

$$\xi_{\max}\,(\xi_{\max}-\xi)+\mathbb{P}\,[\xi_{\max}-\theta]\int_{\xi}^{\xi_{\max}}\left[\frac{n+3}{n+4}\xi_{\max}(\xi_{\max}-\xi')\right]^{3/(n+3)}\mathrm{d}\xi'=\frac{n+4}{n+3}T^{(n+3)}(\xi). \tag{45}$$

Evaluating the integral and simplifying yields

$$\xi_{\max}\,(\xi_{\max}-\xi)+\mathbb{P}\,[\xi_{\max}-\theta]\,\frac{n+3}{n+6}\,(\xi_{\max}-\xi)\left[\frac{n+3}{n+4}\xi_{\max}\,(\xi_{\max}-\xi)\right]^{\frac{3}{n+3}}=\frac{n+4}{n+3}T^{(n+3)}(\xi). \tag{46}$$

Solving explicitly for $T(\xi)$ gives a more accurate approximation, defined as $T_2(\xi)$

$$T_2(\xi)=\left[\frac{n+3}{n+4}\,(\xi_{\max}-\xi)\left(\xi_{\max}+\mathbb{P}\frac{n+3}{n+6}\,(\xi_{\max}-\theta)\left(\frac{n+3}{n+4}\xi_{\max}\,(\xi_{\max}-\xi)\right)^{3/(n+3)}\right)\right]^{1/(n+3)}. \tag{47}$$

This expression allows for a more accurate approximation of the radiation wave front moving through the cold medium. In the next section, $\xi_{\max}$ will be determined and tabulated for various values of $\mathbb{P}$ and θ under both $n=0$ and 3.

Looking at the case when $\mathbb{P} \to 0$, i.e. radiation energy is negligible, equation (47) becomes

$$T_2(\xi) = \left[\frac{n+3}{n+4}\xi_{\max}\left(\xi_{\max} - \xi\right)\right]^{1/(n+3)}, \tag{48}$$

which is identical to $T_1(\xi)$ and the approximation given by Castor [4]. In comparison, Nelson and Reynolds [6] derive a more accurate expression for the approximate wave front.

5. Evaluated the self-similar solution profiles

To obtain solution profiles, $T(\xi)$ and $\xi_{\max}$ for different problems we used the computer software Wolfram `Mathematica 9`. The solution procedure is as follows. We begin with an initial guess for $\xi_{\max}$ and then solve equation (26) using the boundary conditions $T(\xi_{\max} - \delta) = T_2(\xi_{\max} - \delta)$ and $T'(\xi_{\max} - \delta) = T_2'(\xi_{\max} - \delta)$. Then, based on whether $T(0)$ from this solution is greater than or less than 1, we adjust our guess for $\xi_{\max}$. In our case we used $\delta = 10^{-10}$, and the function `NDSolve` and `FindRoot` to integrate the ordinary differential equation and find the converged $\xi_{\max}$. Our calculations using `NDSolve` and `FindRoot` were performed with better-than machine precision arithmetic by setting the parameter `WorkingPrecision` to 32. To verify our solution procedure we computed $\xi_{\max}$ using $\mathbb{P} = 0$ for $n = 0$ and 3 and compared with the results from Nelson and Reynolds. Our solutions agree with theirs to six significant digits.

Using our solutions we can look at the impact of including the radiation energy density terms in a stationary material, i.e. having $\mathbb{P} > 0$ and $\theta = 0$. To do this, we look at a typical Marshak wave solution that has appeared several times in the literature [16, 21, 22]. It has $c_{v\infty} = 0.1\,\mathrm{GJ\,g^{-1}\,keV^{-1}}$, $\rho_\infty = 3.0\,\mathrm{g\,cm^{-3}}$, $\kappa_0 = 300$, $T_\infty = 1.0\,\mathrm{keV}$ and $l = 1\,\mathrm{cm}$. Using these parameters, $\mathbb{C} = 948.027$ and $\mathbb{P} = 0.045\,73$. Based on our solutions for this problem $\xi_{\max} = 1.221\,16$ in the $n = 0$ case and $\xi_{\max} = 1.106\,22$ in the $n = 3$ case. This compares to the 'low $\mathbb{P}$' solution given by Nelson and Reynolds of $\xi_{\max} = 1.231\,17$ in the $n = 0$ case and $\xi_{\max} = 1.119\,93$ in the $n = 3$ case. For both of these the difference is about 1%. As shown in table 1, with no material motion the radiation wave travels slightly slower in the similarity variable ξ (but not necessarily in physical distance x) when $\mathbb{P}$ increases (the radiation energy relative to material energy density increases). Based on numerical results from $\mathbb{P}$ ranging from 0 to 2, we find that, for $\theta = 0$, $\xi_{\max}$ behaves as

$$\xi_{\max} \approx 0.032\mathbb{P}^2 - 0.19\mathbb{P} + 1.231\,17, \quad n = 0, \tag{49}$$

$$\xi_{\max} \approx 0.046\mathbb{P}^2 - 0.25\mathbb{P} + 1.106\,22, \quad n = 3. \tag{50}$$

Note we have not included more decimals in the linear and quadratic coefficients of the model because the least-squares fit indicated that these were the only digits that were significant with respect to the standard error in the coefficients.

In table 1 we also show the effect of having a moving material in the entries having a non-zero θ. It is apparent, as would be expected, that having the material moving toward the right proportional to $t^{-1/2}$ causes the wave to move farther. The effect of material motion is also related to $\mathbb{P}$: the larger the value of $\mathbb{P}$ the farther the wave travels. This is due to the fact that the advection term in equation (26) is scaled by $\mathbb{P}$. In the $\mathbb{P} = 0.045\,73$ case increasing θ to 10 from 0 has about a 15% effect in $\xi_{\max}$ for $n = 3$. The same change at $\mathbb{P} = 1$ leads to over 450% effect in $\xi_{\max}$.

Table 1. ξ_{max} for motion problems.

		ξ_{max}	
$\mathbb{P}$	θ	$n=0$	$n=3$
0.045 73	10	1.364 49	1.282 13
	5	1.288 45	1.189 59
	2	1.247 12	1.138 52
	1	1.233 99	1.122 20
	0.1	1.222 43	1.107 80
	0	1.221 16	1.106 22
0.5	10	3.575 74	3.528 16
	5	2.071 07	2.010 57
	2	1.409 00	1.315 16
	1	1.259 37	1.141 68
	0.1	1.149 10	1.009 25
	0	1.138 06	0.995 82
1	10	5.198 30	5.164 51
	5	2.832 72	2.763 74
	2	1.576 27	1.479 67
	1	1.282 25	1.157 90
	0.1	1.087 84	0.931 03
	0	1.069 66	0.909 32

In figure 1 we show thermal wave profiles for $\mathbb{P} = 0.045\,73$ with $n = 0$ and 3. In these figures we can see the impact of increasing θ discussed above. The value of θ does not appear to affect the steepness of the solution at the wavefront. We did not show the smaller values of θ in these figures because their curves are very close to that for $\theta = 1$.

6. Self-similar solutions for code verification

Above we have explored the impact of including both radiation energy and material motion on the classical Marshak wave problem. We also believe these solutions are useful for test problems for RHD codes. This can be accomplished by making the code fix the material velocity everywhere to have $u(t) = \theta U/\sqrt{t}$ and performing the radiation solve with this prescribed $u(t)$. In principle there could be an issue with evaluating $u(0)$ because of the singularity, but in practice most radiation solvers expect to receive the velocity evaluated at either the end of the time step or some intermediate time level.

To demonstrate this is indeed possible we took an existing radiation solver based on the spherical harmonics approximation for slab geometry problems [16, 23] and ran a problem with $\mathbb{P} = 0.045\,73$ and $\theta = 10$ and $n = 3$. Because the code works in dimensional units we picked $c_{v\infty} = 0.1\,\mathrm{GJ\,g^{-1}\,keV^{-1}}$, $\rho_\infty = 3.0\,\mathrm{g\,cm^{-3}}$, $\kappa_0 = 300$, $T_\infty = 1.0\,\mathrm{keV}$, $n = 3$ and $l = 1\,\mathrm{cm}$. In running the problem we evaluated u at the middle of each time step. The results from this numerical solution are compared with the self-similar profiles computed in the previous section in figure 2. In this figure we show the solution for three different times: 10, 20 and 50 ns.

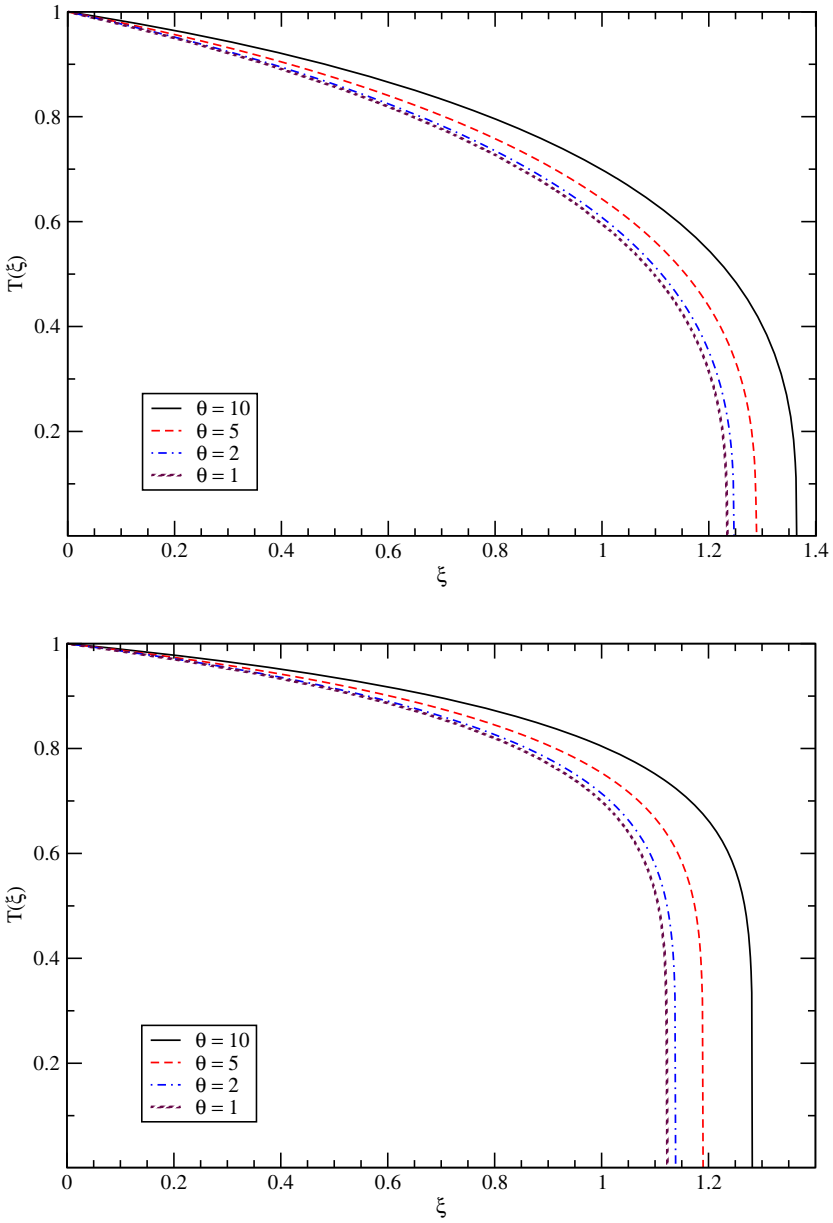

Figure 1. Self-similar thermal wave profiles for $\mathbb{P} = 0.045\,73$ with $n = 0$ (top) and $n = 3$ (bottom).

For illustration of the difference between our solution and that without material motion we have also plotted the solution when $\theta = 0$; this demonstrates that the material motion is noticeably affecting the solution, and if the code did not have any treatment of the relativistic terms in the coupling, the solution would be noticeably different. The numerical solution, obtained using 30 spatial cells and a time step size of 1.6667×10^{-4} ns follows the self-similar profiles very closely.

We also did a simple convergence study for this problem by looking at the relative error at 50 ns between the numerical and semi-analytic solutions at $x = 0.2$ cm as a function of the mesh spacing Δx; see figure 3. Convergence results for a transport code can be misleading because the

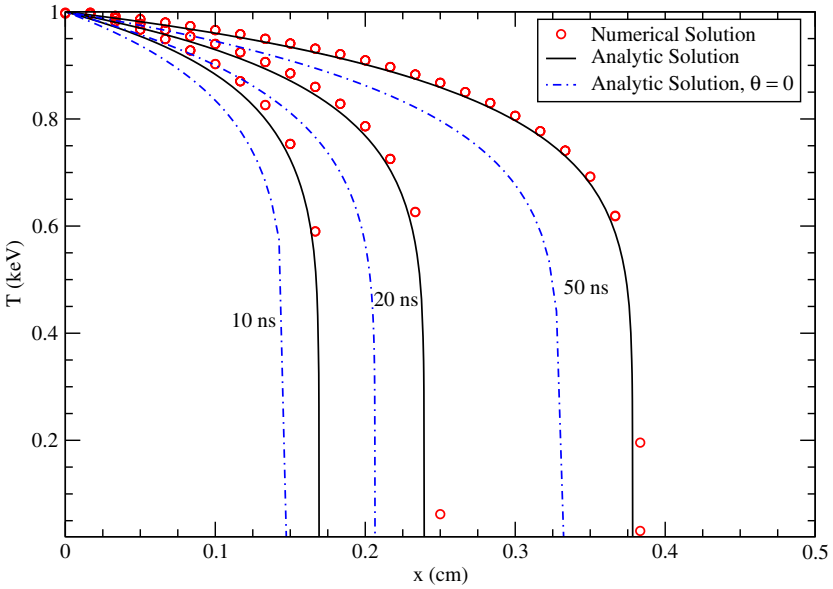

Figure 2. Comparison of numerical solution to analytic self-similar solution to a Marshak-like wave problem that has material motion and non-negligible radiation energy. The $\theta = 0$ curve is the solution without material motion. This problem has a driving temperature of 1 keV, and $\sigma = 300\,T^{-3}\,\mathrm{cm}^{-1}$, and $\rho c_\mathrm{v} = 0.3\ \mathrm{GJ\,cm^{-3}\,keV^{-1}}$.

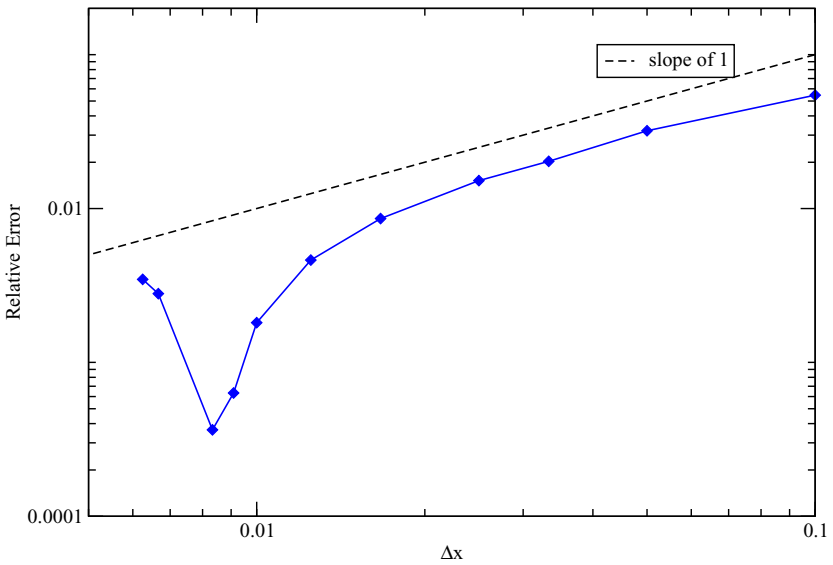

Figure 3. Convergence of the relative error in the Marshak-like wave problem shown in figure 2 at $t = 50$ ns and $x = 0.2$ cm and a Courant–Freidrichs–Lewy number ($\frac{c\Delta t}{\Delta x}$) of 0.3. We observe first-order convergence before the mesh resolution pushes the numerical solution outside the asymptotic drift-diffusion limit. See the text for further discussion.

Table 2. Solutions $T(\xi)$ for a problem with $\mathbb{P} = 0.045\,73$ and $n = 0$.

	ξ	$\theta = 10$	$\theta = 5$	$\theta = 2$	$\theta = 1$	$\theta = 0.1$	$\theta = 0$
1	0.000 00	1.000 00	1.000 00	1.000 00	1.000 00	1.000 00	1.000 00
2	0.028 43	0.995 34	0.994 27	0.993 59	0.993 36	0.993 16	0.993 13
3	0.056 85	0.990 54	0.988 40	0.987 05	0.986 59	0.986 17	0.986 12
4	0.085 28	0.985 62	0.982 39	0.980 35	0.979 66	0.979 03	0.978 96
5	0.113 71	0.980 56	0.976 23	0.973 51	0.972 58	0.971 74	0.971 65
6	0.142 13	0.975 35	0.969 91	0.966 50	0.965 34	0.964 29	0.964 17
7	0.170 56	0.970 00	0.963 44	0.959 33	0.957 93	0.956 67	0.956 52
8	0.198 99	0.964 50	0.956 80	0.951 99	0.950 35	0.948 87	0.948 70
9	0.227 42	0.958 83	0.949 99	0.944 46	0.942 59	0.940 89	0.940 70
10	0.255 84	0.953 00	0.943 00	0.936 75	0.934 64	0.932 72	0.932 51
11	0.284 27	0.947 00	0.935 82	0.928 85	0.926 49	0.924 35	0.924 12
12	0.312 70	0.940 82	0.928 44	0.920 74	0.918 13	0.915 78	0.915 51
13	0.341 12	0.934 45	0.920 86	0.912 41	0.909 56	0.906 98	0.906 69
14	0.369 55	0.927 88	0.913 06	0.903 87	0.900 76	0.897 95	0.897 64
15	0.397 98	0.921 11	0.905 03	0.895 08	0.891 72	0.888 68	0.888 34
16	0.426 40	0.914 12	0.896 77	0.886 04	0.882 42	0.879 15	0.878 78
17	0.454 83	0.906 91	0.888 26	0.876 74	0.872 86	0.869 35	0.868 96
18	0.483 26	0.899 46	0.879 49	0.867 16	0.863 01	0.859 26	0.858 84
19	0.511 68	0.891 76	0.870 43	0.857 29	0.852 87	0.848 87	0.848 42
20	0.540 11	0.883 79	0.861 09	0.847 10	0.842 40	0.838 15	0.837 67
21	0.568 54	0.875 56	0.851 43	0.836 58	0.831 59	0.827 08	0.826 58
22	0.596 97	0.867 02	0.841 43	0.825 71	0.820 42	0.815 64	0.815 11
23	0.625 39	0.858 18	0.831 09	0.814 45	0.808 85	0.803 80	0.803 24
24	0.653 82	0.849 01	0.820 36	0.802 78	0.796 87	0.791 53	0.790 94
25	0.682 25	0.839 48	0.809 23	0.790 67	0.784 43	0.778 80	0.778 17
26	0.710 67	0.829 58	0.797 66	0.778 08	0.771 50	0.765 56	0.764 90
27	0.739 10	0.819 28	0.785 61	0.764 97	0.758 03	0.751 76	0.751 07
28	0.767 53	0.808 55	0.773 06	0.751 29	0.743 97	0.737 36	0.736 63
29	0.795 95	0.797 35	0.759 94	0.736 99	0.729 27	0.722 29	0.721 51
30	0.824 38	0.785 65	0.746 22	0.722 00	0.713 84	0.706 47	0.705 65
31	0.852 81	0.773 41	0.731 82	0.706 24	0.697 62	0.689 83	0.688 96
32	0.881 23	0.760 57	0.716 68	0.689 62	0.680 50	0.672 23	0.671 31
33	0.909 66	0.747 08	0.700 71	0.672 04	0.662 35	0.653 57	0.652 59
34	0.938 09	0.732 87	0.683 80	0.653 35	0.643 03	0.633 67	0.632 62
35	0.966 52	0.717 86	0.665 83	0.633 38	0.622 34	0.612 31	0.611 19
36	0.994 94	0.701 96	0.646 64	0.611 90	0.600 04	0.589 23	0.588 02
37	1.023 37	0.685 06	0.626 03	0.588 64	0.575 80	0.564 05	0.562 74
38	1.051 80	0.667 01	0.603 74	0.563 20	0.549 16	0.536 25	0.534 80
39	1.080 22	0.647 64	0.579 43	0.535 02	0.519 46	0.505 06	0.503 43
40	1.108 65	0.626 72	0.552 62	0.503 29	0.485 70	0.469 25	0.467 38
41	1.137 08	0.603 98	0.522 62	0.466 69	0.446 21	0.426 72	0.424 48
42	1.165 50	0.579 01	0.488 37	0.422 90	0.397 82	0.373 13	0.370 23
43	1.193 93	0.551 27	0.448 08	0.367 05	0.333 01	0.296 52	0.291 96
44	1.222 36	0.519 95	0.398 32	0.284 79	0.220 73	0.041 26	–
45	1.250 78	0.483 78	0.330 76	–	–	–	–
46	1.279 21	0.440 55	0.207 40	–	–	–	–
47	1.307 64	0.385 73	–	–	–	–	–
48	1.336 07	0.306 86	–	–	–	–	–
49	1.364 49	–	–	–	–	–	–

Table 3. Solutions $T(\xi)$ for a problem with $\mathbb{P} = 0.045\,73$ and $n = 3$.

	ξ	$\theta = 10$	$\theta = 5$	$\theta = 2$	$\theta = 1$	$\theta = 0.1$	$\theta = 0$
1	0.000 00	1.000 00	1.000 00	1.000 00	1.000 00	1.000 00	1.000 00
2	0.026 71	0.997 29	0.996 77	0.996 43	0.996 32	0.996 22	0.996 20
3	0.053 42	0.994 52	0.993 46	0.992 79	0.992 55	0.992 34	0.992 32
4	0.080 13	0.991 68	0.990 07	0.989 05	0.988 70	0.988 38	0.988 34
5	0.106 84	0.988 77	0.986 60	0.985 22	0.984 75	0.984 32	0.984 27
6	0.133 56	0.985 79	0.983 05	0.981 30	0.980 70	0.980 16	0.980 10
7	0.160 27	0.982 73	0.979 40	0.977 28	0.976 55	0.975 89	0.975 82
8	0.186 98	0.979 60	0.975 67	0.973 16	0.972 29	0.971 51	0.971 42
9	0.213 69	0.976 38	0.971 83	0.968 92	0.967 92	0.967 01	0.966 91
10	0.240 40	0.973 08	0.967 89	0.964 57	0.963 43	0.962 39	0.962 28
11	0.267 11	0.969 68	0.963 84	0.960 10	0.958 81	0.957 64	0.957 51
12	0.293 82	0.966 19	0.959 67	0.955 49	0.954 06	0.952 75	0.952 60
13	0.320 53	0.962 61	0.955 38	0.950 75	0.949 16	0.947 71	0.947 55
14	0.347 24	0.958 91	0.950 97	0.945 87	0.944 12	0.942 52	0.942 34
15	0.373 96	0.955 11	0.946 42	0.940 83	0.938 91	0.937 16	0.936 96
16	0.400 67	0.951 19	0.941 72	0.935 63	0.933 54	0.931 62	0.931 41
17	0.427 38	0.947 15	0.936 87	0.930 26	0.927 98	0.925 89	0.925 66
18	0.454 09	0.942 98	0.931 86	0.924 70	0.922 22	0.919 96	0.919 71
19	0.480 80	0.938 67	0.926 68	0.918 93	0.916 26	0.913 81	0.913 54
20	0.507 51	0.934 21	0.921 31	0.912 96	0.910 07	0.907 43	0.907 13
21	0.534 22	0.929 60	0.915 74	0.906 75	0.903 64	0.900 79	0.900 47
22	0.560 93	0.924 83	0.909 96	0.900 29	0.896 94	0.893 87	0.893 53
23	0.587 64	0.919 87	0.903 94	0.893 56	0.889 96	0.886 65	0.886 28
24	0.614 35	0.914 73	0.897 67	0.886 53	0.882 66	0.879 10	0.878 70
25	0.641 07	0.909 38	0.891 14	0.879 18	0.875 01	0.871 19	0.870 76
26	0.667 78	0.903 81	0.884 30	0.871 47	0.866 99	0.862 87	0.862 40
27	0.694 49	0.898 00	0.877 14	0.863 36	0.858 54	0.854 10	0.853 60
28	0.721 20	0.891 93	0.869 62	0.854 81	0.849 62	0.844 82	0.844 29
29	0.747 91	0.885 58	0.861 70	0.845 77	0.840 16	0.834 98	0.834 40
30	0.774 62	0.878 93	0.853 35	0.836 17	0.830 11	0.824 49	0.823 86
31	0.801 33	0.871 93	0.844 49	0.825 94	0.819 36	0.813 25	0.812 57
32	0.828 04	0.864 56	0.835 08	0.814 98	0.807 82	0.801 15	0.800 39
33	0.854 75	0.856 78	0.825 03	0.803 18	0.795 34	0.788 01	0.787 18
34	0.881 47	0.848 52	0.814 24	0.790 37	0.781 74	0.773 64	0.772 72
35	0.908 18	0.839 75	0.802 60	0.776 37	0.766 79	0.757 75	0.756 72
36	0.934 89	0.830 38	0.789 95	0.760 89	0.750 15	0.739 94	0.738 77
37	0.961 60	0.820 32	0.776 08	0.743 58	0.731 37	0.719 65	0.718 30
38	0.988 31	0.809 48	0.760 72	0.723 88	0.709 73	0.695 95	0.694 35
39	1.015 02	0.797 70	0.743 48	0.700 94	0.684 08	0.667 29	0.665 31
40	1.041 73	0.784 81	0.723 79	0.673 35	0.652 35	0.630 63	0.628 01
41	1.068 44	0.770 58	0.700 78	0.638 37	0.610 10	0.578 49	0.574 45
42	1.095 15	0.754 67	0.672 93	0.589 60	0.544 24	0.478 72	0.468 07
43	1.121 87	0.736 61	0.637 34	0.503 00	0.262 30	–	–
44	1.148 58	0.715 69	0.586 96	–	–	–	–
45	1.175 29	0.690 73	0.493 28	–	–	–	–
46	1.202 00	0.659 64	–	–	–	–	–
47	1.228 71	0.617 87	–	–	–	–	–
48	1.255 42	0.551 97	–	–	–	–	–
49	1.282 13	0.018 24	–	–	–	–	–

diffusion limit is only an asymptotic limit of the full transport system. In this problem the scaling parameter ϵ is on the order of 10^{-1} and once the mesh and time step start to resolve a mean-free path or the mean-free time, the numerical method no longer is equivalent to the asymptotic drift-diffusion equation. Therefore, we expect that beyond some level of resolution, the solution will no longer converge to the self-similar profile we obtained. This is evident in our results: below a certain mesh resolution the error begins to increase. Before this point we do observe first-order convergence as we would expect for a problem with a non-smooth solution. We know of no prior work on the correct behavior of transport numerical methods in the transition region between the drift-diffusion limit. It is well known, however, that if a numerical method did not possess the proper diffusion limit, the solution would not show convergence until a mean-free path was resolved (see, for instance, [23]).

To allow other to use these solutions for code verification we have included $T(\xi)$ for various values θ at $\mathbb{P} = 0.045\,73$ in tables 2 and 3.

7. Conclusion

We have generalized the classic Marshak wave problem to include both radiation energy density terms and material motion. The material motion in our solutions is uniform in space and proportional to $t^{-1/2}$. In problems without any material motion, we observe that the greater the radiation energy density, as measured by the parameter $\mathbb{P}$, the slower the wave moves with respect to the similarity variable ξ. We phenomenologically quantified this effect with a quadratic in $\mathbb{P}$ model. Besides providing insight into the effects of radiation energy and material motion on Marshak waves, our solution can also be used to verify the radiation–material coupling treatment in a simulation code.

References

[1] Marshak R E 1958 Effect of radiation on shock wave behavior *Phys. Fluids* **1** 24–9
[2] Petschek A G, Williamson R E and Wooten J K Jr 1960 Penetration of radiation with constant driving temperature *Technical Report* LAMS-2421 Los Alamos Scientific Laboratory
[3] Drake R P 2006 *High Energy Density Physics* (New York: Springer)
[4] Castor J 2004 *Radiation Hydrodynamics* (Cambridge: Cambridge University Press)
[5] Zel'dovich Ya B and Raizer Yu P 2002 *Physics of Shock Waves and High-Temperature Hydrodynamic Phenomena* (Mineola: Dover)
[6] Nelson E M and Reynolds J 2009 Semi-analytic solution for a Marshak wave via numerical integration in mathematica *Technical Report* Los Alamos Scientific Laboratory
[7] Coggeshall S V and Axford R A 1986 Lie group invariance properties of radiation hydrodynamics equations and their associated similarity solutions *Phys. Fluids* **29** 2398–2420
[8] Lowrie R B and Rauenzahn R M 2007 Radiative shock solutions in the equilibrium diffusion limit *Shock Waves* **16** 445–53
[9] Lowrie R B and Edwards J D 2008 Radiative shock solutions with grey nonequilibrium diffusion *Shock Waves* **18** 129–43
[10] McClarren R G, Paul Drake R, Morel J E and Holloway J P 2010 Theory of radiative shocks in the mixed, optically thick–thin case *Phys. Plasmas* **17** 093301
[11] Drake R P 2007 Energy balance, and structural regimes of radiative shocks in optically thick media *IEEE Trans. Plasma Sci.* **35** 171–80
[12] Drake R P 2007 Theory of radiative shocks in optically thick media *Phys. Plasmas* **14** 043301

[13] Morel J E 2000 Diffusion-limit asymptotics of the transport equation, the $P_{1/3}$ equations, and two flux-limited diffusion theories *J. Quantitative Spectrosc. Radiat. Transfer* **65** 769–78
[14] Densmore J D and Larsen E W 2004 Asymptotic equilibrium diffusion analysis of time-dependent Monte Carlo methods for gray radiative transfer *J. Comput. Phys.* **199** 175–204
[15] Adams M L and Nowak P F 1998 Asymptotic analysis of a computational method for time- and frequency-dependent radiative transfer *J. Comput. Phys.* **146** 366–403
[16] McClarren R G, Evans T M, Lowrie R B and Densmore J D 2008 Semi-implicit time integration for P_N thermal radiative transfer *J. Comput. Phys.* **227** 7561–86
[17] Lowrie R B and Morel J E 2001 Issues with high-resolution Godunov methods for radiation hydrodynamics *J. Quantitative Spectrosc. Radiat. Transfer* **69** 475–89
[18] McClarren R G, Holloway J P and Brunner T A 2008 On solutions to the P_n equations for thermal radiative transfer *J. Comput. Phys.* **227** 2864–85
[19] Larsen E W, Pomraning G C and Badham V C 1983 Asymptotic analysis of radiative transfer problems *J. Quantitative Spectrosc. Radiat. Transfer* **29** 285–310
[20] Pomraning G C 1979 The non-equilibrium Marshak wave problem *J. Quantitative Spectrosc. Radiat. Transfer* **21** 249–61
[21] Edwards J D, Morel J E and Knoll D A 2011 Nonlinear variants of the TR/BDF2 method for thermal radiative diffusion *J. Comput. Phys.* **230** 1198–214
[22] Larsen E W, Kumar A and Morel J E 2013 Properties of the implicitly time-differenced equations of thermal radiation transport *J. Comput. Phys.* **238** 82–96
[23] McClarren R G and Lowrie R B 2008 The effects of slope limiting on asymptotic-preserving numerical methods for hyperbolic conservation laws *J. Comput. Phys.* **227** 9711–26